Solid Earth Discuss., 5, 1641–1657, 2013
www.solid-earth-discuss.net/5/1641/2013/
doi:10.5194/sed-5-1641-2013

Solid Earth
Discussions
Open Access

Seismic structure of the lithosphere beneath the ocean islands near the mid-oceanic ridges

C. Haldar, P. Kumar, and M. Ravi Kumar

National Geophysical Research Institute (CSIR), Uppal Road, Hyderabad-500007, India

Received: 4 September 2013 – Accepted: 13 September 2013 – Published: 7 October 2013

Correspondence to: P. Kumar (prakashk@ngri.res.in)

Published by Copernicus Publications on behalf of the European Geosciences Union.

Abstract

Deciphering the seismic character of the young lithosphere near the mid-oceanic ridges (MOR) is a challenging endeavor. In this study, we determine the seismic structure of the oceanic plate near the MORs, using the *P*-to-*s* conversions isolated from good quality data recorded at 5 broadband seismological stations situated on the ocean Islands in their vicinity. Estimates of the crustal and lithospheric thickness values from waveform modeling of the *P* receiver function stacks reveal that the crustal thickness varies between 6 and 8 km with the corresponding depths to the lithosphere asthenosphere boundary (LAB) varying between 43 and 68 km. However, the depth to the LAB at Macquire Island is intriguing in view of the observation of a thick (~ 87 km) lithosphere beneath a relatively young crust. At three other stations i.e., Ascension Island, Sao Jorge and Easter Island, we find evidence for an additional deeper low velocity layer probably related to the presence of a hotspot.

1 Introduction

The Mid-Oceanic Ridges (MOR) are the largest sources of magma on the earth. Being locales where new lithosphere is generated and accreted to the existing ones, their study assumes importance in understanding the dynamics of plate tectonics. These linear features on the ocean floor control the rheology of oceanic lithosphere, ridge topography, the style of oceanic crustal accretion and also affect the earth's deeper discontinuities. New oceanic plates created at the mid-oceanic ridges undergo cooling and thickening as they subsequently spread away and again plunge downward into the mantle along the trenches by the process of subduction. In a broader perspective, the thermal contraction of lithosphere created at the ridge also defines the shape of the mid-oceanic ridge (Parsons and Scalater, 1977). The lithosphere is the rigid outer shell, made up of the crust and the top most part of the mantle that floats over a lower viscosity asthenosphere that is seismically characterized by a low velocity zone.

SED
5, 1641–1657, 2013

The first seismic observation of the asthenospheric low velocity layer was reported by Gutenberg, at a depth range of ~ 50–200 km (Gutenberg, 1959). Therefore, any velocity reduction in the uppermost mantle, similar to the one at LAB, has been sometimes referred to as the Gutenberg (G) discontinuity (Revenaugh and Jordan, 1991), which may define the top of the low-velocity layer. At short scales, the lithosphere is deformed due to faults (Atwater and Mudie, 1968; Ballard and Van Andel, 1977).

Most of the seismological knowledge of the oceanic plates, particularly that near the ridges comes from tomography studies (Evangelidis et al., 2004; Rodgers and Harben, 1999) with the exception of a few seismic reflection/refraction studies that have been carried out across the ridges (Du and Foulger, 1999; Bjarnson and Menke, 1993; Evangelidis et al., 2004; Rodgers and Harben, 1999). Surface wave dispersion studies first elucidated the nature of the oceanic plate and LAB (Kanamori and Press, 1970; Leeds, 1975; Zhang and Tanimoto, 1993; Nettles and Dziewonski, 2008). However, the depth resolution of surface wave and body wave tomography studies is limited to > 40 km. Shear-wave anisotropy studies suggest horizontally connected melts near the MOR (Nowaki et al., 2012). Attempts to understand the oceanic plates have been made through a number of seismological studies at different locations beneath the Pacific ocean (Gaherty, 1999; Tan and Helmberger, 2007; Kawakatsu, 2009; Kumar and Kawakatsu, 2011; Kumar et al., 2012; Rychert and Shearer, 2011; Schmerr, 2012 etc). Logistic problems and the extreme costs compared to land surveys, impose severe constraints on obtaining similar information about the nature of other MORs. Another factor which hampers body wave observations from the oceanic data is the water reverberations that mostly contaminate the vertical component of the seismograms of the ocean bottom seismometers (Kumar et al., 2012). In this study, an attempt is made to investigate the seismic structure using the available data from 5 seismological stations situated on the islands but close to the mid-oceanic ridges. Although the crustal structure may not truly represent the nature of the oceanic plate due to possible influence of the islands, the deeper structure is devoid of such effects.

SED
5, 1641–1657, 2013

2 Data and methods

We used all the available teleseismic data from five oceanic islands near the MORs. The locations of the stations are shown in Fig. 1 together with the major plate boundary and mid-oceanic ridges. In the present study, we use converted wave techniques, namely *P* receiver functions (PRF) (Burdick and Langston, 1977; Langston, 1977; Vinnik, 1977). Receiver functions are time series, computed from three component seismograms, which show the relative response of Earth structure near the receiver. The events with magnitude ≥ 5.5 Mb and epicentral distance range of 30–90° are selected from all available back azimuths. First, the *Z*, *N* and *E* components are rotated into *Z*(vertical), *R*(radial), and *T*(transverse) system using back azimuths derived from the waveforms. We further rotate the *ZRT* components into the LQT system using the theoretical angle of incidence determined by the global velocity model, IASP91 and also with the angle of maximum polarization direction of *P* wave. We chose only those events whose difference in theoretical and waveform back-azimuth and incidence angle are less than 30° and 5° respectively. Further, we derive the *P* receiver functions in time domain by deconvolving the radial components by their respective vertical ones. The deconvolution makes the equalization of source and propagation path effects. *P* receiver functions thus obtained are then moveout corrected to a reference slowness of 6.4 s deg^{-1} (Yuan, 1997) in order to remove the dependence of the travel times of the converted phases on the source receiver distance. In addition, we stack several *P* receiver functions after moveout correction, to enhance the signal to noise ratio.

3 Results and discussion

The receiver function results are summarized in the Table 1 and the observed stacked traces are shown in Fig. 2. In order to pick the conversions unambiguously, we perform error analysis utilizing the bootstrap technique (Efron and Tibshirani, 1993) and consider only those phases which are above ±2 SE error bound. In Fig. 2, the stacked

SED
5, 1641–1657, 2013

P receiver functions for the corresponding stations are shown. The prominent discontinuities are marked. The phases observed prior to ~3 s are interpreted as Ps conversions from the Moho, which are positive in polarity arising due to the increase in velocity downward. Other discontinuities which are marked as LVL (low velocity layer) and LAB (Lithosphere-Asthenosphere Boundary) are also visible above the error limit. Further, we generate synthetics (Frederiksen and Bostock, 1999) using simple models in order to constrain the depths to the boundaries. The 1-D synthetic *P*-to-*s* receiver functions for each of the stations are shown by dashed wiggles (Fig. 2) and the corresponding models are shown in Fig. 3. Since the islands are volcanic in nature, the velocities and crustal thickness values are taken from other studies to construct the upper crustal models. While modeling the RFs at various stations, the velocity of the basaltic layer was adopted from Rodgers and Harben (1999). Also the velocities in the crustal part are kept close to the estimates obtained regionally and globally based on active seismic experiments (Shinohara, 2008; White, 1992), except for the station PSCM where the data required inclusion of a low velocity layer at the top.

3.1 Mid-Atlantic ridge (PSCM, ROSA and ASCN)

These three stations are located in the Atlantic ocean; PSCM and ROSA are in the north Atlantic and station ASCN is located in the central part (Fig. 1). The station PSCM is at the Terceira Island while ROSA is at Sao Jorge Island in the middle of the North Atlantic Ocean. Both these islands are volcanic in origin and about 10 km away from the MOR, making it one of the closest landmasses to an active, oceanic spreading center. ASCN is located in the South Atlantic Ocean at Ascension Island, which is a volcanic island. This island is located 100 km west of the MOR.

Our modeling results indicate that the crust-mantle boundary is located at depths of ~6, 7 and 8 km for ROSA, PSCM and ASCN respectively. Near the station ASCN, the wide-angle reflection seismic tomography studies indicate the Moho depth at ~10.2 km (Evangelidis et al., 2004). The depths to the LAB beneath these stations are at 40, 68 and 48 km respectively. The result for the station ASCN is consistent with the observa-

SED
5, 1641–1657, 2013

tions by Li et al. (2003b). The depth to the LAB beneath ROSA (~ 40 km) and PASCM (~ 68 km) are quite different, in spite of the fact that they are only ~ 100 km apart with similar average crustal ages (the average crustal ages of ROSA and PSCM are 13 and 19 My respectively). The inset of Fig. 1 shows that PSCM much closer to the ridge compared to ROSA. These two stations are situated on a complex triple junction ridge system. The possible reason for this discrepancy might be due to the influence of the compositional nature of the oceanic islands and structural complexity.

3.2 Rano Kau ridge (RPN) and Macquarie ridge (MCQ)

Station RPN is situated at the Easter Island, ~ 100 km west from the Rano Kau Ridge in the Pacific, while station MCQ is located at the Macquarie Island, which lies in the middle of the Macquarie Ridge. Both these volcanic islands are dominated by the presence of basalt and gabbro. The results of receiver function modeling suggest a crustal thickness of ~ 7 km and plate thickness of 43 km at station RPN. On the other hand, the crust (~ 24 km thick) and the lithosphere are much thicker (~ 87 km) below station MCQ. The LAB depth found below RPN is consistent with the results obtained earlier from *S* receiver functions (Heit et al., 2007; Li, et al., 2003b). This study suggests that the numerical value corresponding to the negative discontinuity below RPN might correspond to a oceanic LAB.

4 Upper mantle discontinuities

Figure 4 shows the receiver function stacks at individual stations after application of a low-pass filter with a corner frequency of 6 s. The stacks clearly reveal the global upper mantle seismic discontinuities typically detected at 44.1 and 68.1 s. However, the oceanic stations reveal a delay in both the phases (see Table 1). These seismic discontinuities are globally observed and generally interpreted to be formed due to a phase transformation in the mantle from olivine to spinel and from spinel-structured

SED
5, 1641–1657, 2013

gamma phase to perovskite-structured magnesiowustite (Duffy and Anderson, 1989) respectively. These phases are in a state of equilibrium governed by the temperature and pressure at those depths, described by the Clayperon slope. The Clayperon slope is positive and negative for the 410 and 660 km discontinuities respectively. Thus, the respective locations of these phases can be interpreted in terms of the temperature in the upper mantle. For an excess temperature of ∼200 °C, the separation between these discontinuities can be reduced by ∼20–30 km (Helffrich, 2000). The delays in both the phases might also indicate the lower average velocity in the upper mantle implying a thinner mantle-lid of the oceanic lithosphere as compared to the continental mantle.

The arrival times for the upper-mantle discontinuities are listed in the Table 1. All the stations show delay in both the discontinuities with respect to the global average value predicted by the IASP91 model. These observed delays might be related to elevated upper-mantle temperatures just below the mid-oceanic ridges where hot magmas are continuously out poured to make new lithosphere. These values are in general agreement with the earlier results in oceanic environments by receiver function analysis (Li et al., 2003a) and SS-precursors (Gu and Dziewonski, 2002). The observed values suggest that the thickness of the upper mantle transition zone varies between 227 and 248 km as compared to the global average value of ∼250 km. This thinning of the transition zone favors a hotter mantle (e.g Agee, 1997; Shearer, 2000; Deuss, 2007).

5 Low velocity layer

The observed receiver function traces (Fig. 2) show an additional negative phase for stations RPN, ROSA and ASCN. We choose to interpret the shallower LVLs as conversions from LAB, since they are consistent with previous studies using different seismological techniques (Heit et al., 2007; Rychert and Shearer, 2009 etc.) and also these values are close to those predicted by the cooling model for ocean lithosphere. The deeper low velocity layers (Fig. 2) below RPN, ROSA and ASCN are observed much

SED
5, 1641–1657, 2013

beyond the error limits. Owing to the proximity of these stations to the mid-oceanic ridges, the possible source for the generation of these second LVLs may be related to the source of magma at a depth range of ∼75–100 km from where the magma ascends along the narrow lithospheric openings. This observation also get support from the shear wave anisotropy study which argues for the horizontal layers of connected melt pockets in the region near to ridge (Nowacki et al., 2012). The mid-oceanic ridges receive magma from the plume which feed the hot magma from below and the most volatile magmas reside at deeper depths. These locations are where the MORs interact with the mantle plume (Montagner and Ritsema, 2001) and possibly produce the second LVL, as observed along the mid-Atlantic ridge, where regions affected by the shallow mantle plumes are detected, with the exception of Iceland.

6 Conclusions

P receiver function analysis at 5 stations located near the mid ocean ridges reveals significant converted energy from the crust-mantle boundary, LAB and an additional deeper low velocity layer. Modeling results reveal that the Moho depths vary from ∼6 km to ∼8 km except for station MCQ (where it is ∼24 km). Hence, we conclude that the crustal thickness beneath the MORs is ∼8 km. The LAB depths beneath the MORs vary from ∼40 km to ∼92 km. The observed LAB depths are consistent with the thermal cooling model (Stein and Stein, 1992), however, the depth estimates may not represent a pure oceanic plate in view of the contamination from the composition of the ocean islands on which the stations are sited. Further, we observe sufficient converted energy from the upper mantle discontinuities namely the 410 and the 660. These phases are observed at ∼46 s and ∼67 s implying delay with respect to the global average. Also the thickness of the transition zone is found to be thin, due to a deepening of the 410 and swallowing of the 660 km discontinuities. This thinning of the transition zone indicates the existence of mantle plumes beneath the stations (e.g.,

SED
5, 1641–1657, 2013

ASCN and RPN). These findings are very much coherent with the fact that the present observations are in the close vicinity of the mid-oceanic ridges.

Acknowledgements. Seismic data are from IRIS, DMC. Seismic data analysis was performed in Seismic Handler (K. Stammler). Plots are generated using Generic Mapping Tool (Wessel and Smith, 1995). Thanks to Rainer Kind for his valuable suggestions on the initial version of the manuscript. Thanks to M. K. Sen, Director NGRI for giving permission to publish this work. Chinmay Haldar is a Ph.D. student funded by the University Grants Commission (UGC). This work has been performed under the GENIAS Project PSC0104 (PK) of CSIR-NGRI. We thank the Topical Editor, J. Plomerova for constructive suggestions and excellent handling of the manuscript.

References

Agee, C. B.: Phase transformations and seismic structure in the upper mantle and transition zone, in: Ultrahigh-Pressure Mineralogy: Physics And Chemistry of the Earth's Deep Interior, edited by: Hemley, R. J., Reviews in Mineralogy, Mineralogical Society of America, Washington DC, 37, 165–201, 1997.

Atwater, T. and Mudie, J. D.: Block faulting on the Gorda Rise, Science, 159, 729–731, 1968.

Backus, G. E.: Long-wave elastic anisotropy produced by horizontal layering, J. Geophys. Res., 67, 4427–4440, 1962.

Ballard, R. D. and Van Andel, T. H.: Morphology and tectonics of the inner rift valley at lat. 36°50′ N on the Mid-Atlantic Ridge, Geol. Soc. Am. Bull., 88, 507–530, 1977.

Barclay, A. H. and Toomey, D. R.: Shear wave splitting and crustal anisotropy at the Mid-Atlantic Ridge, 35° N, J. Geophys. Res, 108, 2378, doi:10.1029/2001JB000918, 2003.

Bjarnason, I., Menke, W., Flovenz, O., and Caress, D.: Tomographic image of the spreading center in southern Iceland, J. Geophys. Res., 98, 6607–6622, 1993.

Burdick, L. J. and Langston, C. A.: Modelling crustal structure through the use of converted phases in teleseismic body wave forms, B. Seismol. Soc. Am., 67, 677–691, 1977.

Deuss, A.: Seismic observations of transition zone discontinuities beneath hotspot locations, Geol. Soc. Am., 430, 121–136, 2007.

Du, Z. J. and Foulger, G. R.: The crustal structure beneath the northwest fjords, Iceland, from receiver functions and surface waves, Geophys. J. Int., 139, 419–432, 1999.

SED
5, 1641–1657, 2013

Duffy, T. S. and Anderson, D. L.: Seismic velocities in mantle minerals and the mineralogy of the upper mantle, J. Geophys. Res., 94, 1895–1912, 1989.
Efron, B. and Tibshirani, R.: An Introduction to the Bootstrap, Stanford University, California, USA, 1993.
Evangelidis, C. P., Minshull, T. A., and Henstock, T. J.: Three-dimensional crustal structure of Ascension Island from active source seismic tomography, Geophys. J. Int., 159, 311–325, 2004.
Frederiksen, A. W. and Bostock, M. G.: Modelling teleseismic waves in dipping anisotropic structures, Geophys. J. Int., 141, 401–412, 2000.
Gaherty, J. B., Kato, M., and Jordan, T. H.: Seismological structure of the upper mantle: a regional comparison of seismic layering, Phys. Earth Planet. In., 110, 21–41, 1999.
Gu, Y. J. and Dziewonski, A. M.: Global variability of transition zone thickness, J. Geophys. Res., 107, 2135, doi:10.1029/2001JB000489, 2002.
Gutenberg, B.: Physics of the Earth's Interior, Academic Press, New York, 1959.
Heit, B., Sodoudi, F., Yuan, X., Bianchi, M., and Kind, R.: An S receiver function analysis of the lithospheric structure in South America, Geophys. Res. Lett., 34, L14307, doi:10.1029/2007GL030317, 2007.
Helffrich, G.: Topography of the transition zone seismic discontinuities, Rev. Geophys., 38, 141–158, 2000.
Holtzman, B. K.: Melt segregation and strain partitioning: implications for seismic anisotropy and mantle flow, Science, 301, 1227–1230, 2003.
Kanamori, H. and Press, F.: How thick is the lithosphere?, Nature, 226, 330–331, 1970.
Katz, R. F., Spiegelman, M., and Holtzman, B.: The dynamics of melt and shear localization in partially molten aggregates, Nature, 442, 676–679, 2006.
Kawakatsu, H., Kumar, P., Takei, Y., Shinohara, M., Kanazawa, T., Araki, E., and Suyehiro, K.: Seismic evidence for sharp lithosphere-asthenosphere boundaries of oceanic plates, Science, 324, 499–502, 2009a.
Kendall, J. M.: Teleseismic arrivals at a mid-ocean ridge: effects of mantle melt and anisotropy, Geophys. Res. Lett., 21, 301–304, 1994.
Kind, R., Yuan, X., and Kumar, P.: Seismic receiver functions and lithosphere-asthenosphere Boundary, Tectonophysics, 536, 25–43, 2012.

SED
5, 1641–1657, 2013

Kumar, P. and Kawakatsu, H.: Imaging the seismic lithosphere-asthenosphere boundary of the oceanic plate, Geochem. Geophys. Geosyst., 12, Q01006, doi:10.1029/2010GC003358, 2011.

Kumar, P., Kawakatsu, H., Shinohara, M., Kanazawa, T., Araki, E., and Suyehiro, K.: P and S receiver function analysis of seafloor borehole broadband seismic data, J. Geophys. Res., 116, B12308, doi:10.1029/2011JB008506, 2011.

Langston, C. A.: Corvallis, Oregon, crustal and upper mantle structure from teleseismic P and S waves, B. Seismol. Soc. Am., 67, 713–724, 1977.

Leeds, A. R.: Lithospheric thickness in the western Pacific, Phys. Earth Planet. In., 11, 61–64, 1975.

Li, A., Forsyth, D. W., and Fischer, K. M.: Shear velocity structure and azimuthal anisotropy beneath eastern North America from Rayleigh wave inversion, J. Geophys. Res., 10, 2362, doi:10.1029/2002JB002259, 2003a.

Li, X., Kind, R., and Yuan, X.: Seismic study of upper mantle and transition zone beneath hotspots, Phys. Earth Planet. In., 136, 79–92, 2003b.

Menke, W., Brandsdottir, B., Jakobsdottir, S., and Stefansson, R.: Seismic anisotropy in the crust at the Mid-Atlantic plate boundary in south-west Iceland, Geophys. J. Int., 119, 783–790, 1994.

Montagner, J. P. and Ritsema, J.: Interactions between ridges and plumes, Science, 294, 1472–1473, 2001.

Nettles, M. and Dziewo'nski, A.: Radially anisotropic shear velocity structure of the upper mantle globally and beneath North America, J. Geophys. Res.-Sol. Ea., 113, B02303, doi:10.1029/2006JB004819, 2008.

Nowacki, A., Kendall, J. M., and Wookey, J.: Mantle anisotropy beneath the Earth's mid-ocean ridges, Earth Planet. Sc. Lett., 317–318, 56–67, 2012.

Parsons, B. and Sclater, J. G.: An analysis of the variation of ocean floor bathymetrya nd heat flow with age, J. Geophys. Res., 82, 803–827, 1977.

Revenaugh, J. and Jordan, T. H.: Mantle layering from reverberations: 2. The transition zone, J. Geophys. Res., 96, 19763–19780, 1991a.

Rodgers, A. and Harben, P.: Modeling the Conversion of Hydroacoustic to Seismic Energy at Islands and Continental Margins: Preliminary Analysis of Ascension Island Data, 21st Seismic Research Symposium, Technologies for Monitoring the Comprehensive Nuclear-Test-Ban Treaty Las Vegas, Nevada, 1999.

SED
5, 1641–1657, 2013

Rychert, C. A. and Shearer, P. M.: A global view of the lithosphere–asthenosphere boundary, Science, 324, 495–498, 2009.
Rychert, C. A. and Shearer, P. M.: Imaging the lithosphere-asthenosphere boundary beneath the Pacific using SS waveform modeling, J. Geophys. Res., 116, B07307, doi:10.1029/2010JB008070, 2011.
Schmerr, N.: The Gutenberg discontinuity: melt at the lithosphere-asthenosphere boundary, Science, 335, 1480–1483, 2012.
Shearer, P. M.: Upper Mantle Seismic Discontinuities, American Geophysical Union, 115–131, 2000.
Shinohara, M., Fukano, T., Kanazawa, T., Araki, E., Suyehiro, K., Mochizuki, M., Nakahigashi, K., Yamada, T., and Mochizuki, K.: Upper mantle and crustal seismic structure beneath the Northwestern Pacific Basin using seafloor borehole broadband seismometer and ocean bottom seismometers, Phys. Earth Planet. In., 170, 95–106, 2008.
Stein, C. A. and Stein, S.: A model for the global variation in oceanic depth and heat flow with lithospheric age, Nature, 359, 123–129, 1992.
Tan, Y. and Helmberger, D. V.: Trans-Pacific upper mantle shear velocity structure, J. Geophys. Res., 112, B08301, doi:10.1029/2006JB004853, 2007.
Vinnik, L. P.: Detection of waves converted from P to SV in the mantle, Phys. Earth Planet. In., 15, 294–303, 1977.
White, R. S., McKenzie, D., and Onions, R. K.: Oceanic crustal thickness from seismic measurements and rare earth element inversions, J. Geophys. Res., 97, 19683–19715, 1992.
Yaun, X., Ni, J., Kind, R., Mechie, J., and Sandvol, E.: Lithospheric and upper mantle structure of southern Tibet from a seismological passive source experiment, J. Geophys. Res., 102, 27491–27500, 1977.
Zhang, Y. and Tanimoto, T.: High resolution global upper mantle structure and plate tectonics, J. Geophys. Res, 98, 148–227, 1993.

SED
5, 1641–1657, 2013

Table 1. The Moho, LAB, LVL depths beneath the stations used in this study, together with the *P*-to-*s* conversion times from the upper mantle discontinuities. The 2 sigma uncertainties in these values are also indicated.

Station	Region	traces	Moho (km)	LAB ± SE (km)	LVL (km)	410 ± SE (s)	660 ± SE (s)	Age (My)
ASCN	Ascension Island, Atlantic Ocean	20	8 ± 1	48 ± 4	75 ± 4	46.2 ± 0.5	69.0 ± 0.7	5
MCQ	Macquarie Island, Pacific Ocean	15	24 ± 1	87 ± 2	–	48.2 ± 0.5	70.0 ± 0.7	3
PSCM	Terceira Island, Atlantic Ocean	7	7 ± 1	68 ± 7	–	47.8 ± 0.4	71.2 ± 0.5	19
ROSA	Sao Jorge Island, Atlantic Ocean	18	6 ± 1	40 ± 4	100 ± 4	46.8 ± 0.7	70.6 ± 0.7	13
RPN	Easter Island, Pacific Ocean	87	7 ± 1	43 ± 2	76 ± 2	46.2 ± 0.3	68.0 ± 0.3	6

SED
5, 1641–1657, 2013

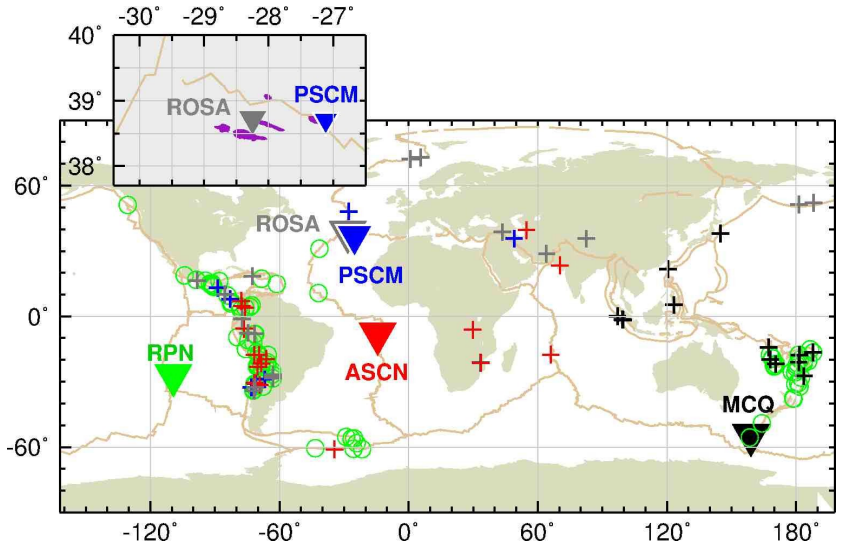

Fig. 1. The location of the seismic stations (inverted triangles) used in the present study. Black line shows the mid-oceanic ridge (MOR) boundary. The color code of the stations corresponds to the colors of the wiggles in the Fig. 2. The crosses and open circles indicate the geographical distribution of the events corresponding to the the stations in the same color. Two stations ROSA and PSCM in north-Atlantic ridge are shown in the zoomed version as inset.

SED
5, 1641–1657, 2013

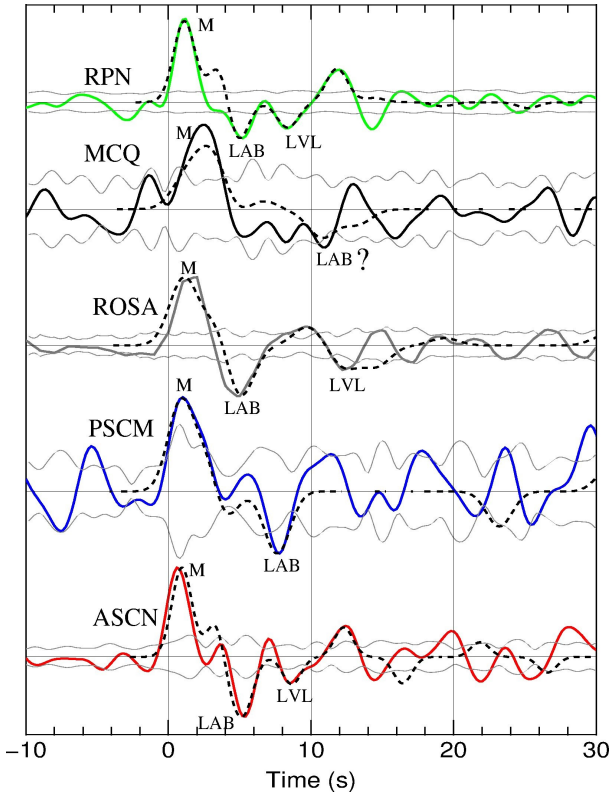

Fig. 2. The observed stacked *P* receiver functions (solid wiggles) from 5 stations are shown. The synthetic *P* receiver functions are also shown by dashed lines for the corresponding models shown in Fig. 3. These receiver functions are filtered with a low pass filter with corner frequency of 0.25 Hz and moveout correction with reference slowness 6.4 s deg^{-1} using the IASP91 Earth model before stacking. The two gray lines on both sides of the mean lines are the standard error estimated using bootstrap for ±2 SE.

SED
5, 1641–1657, 2013

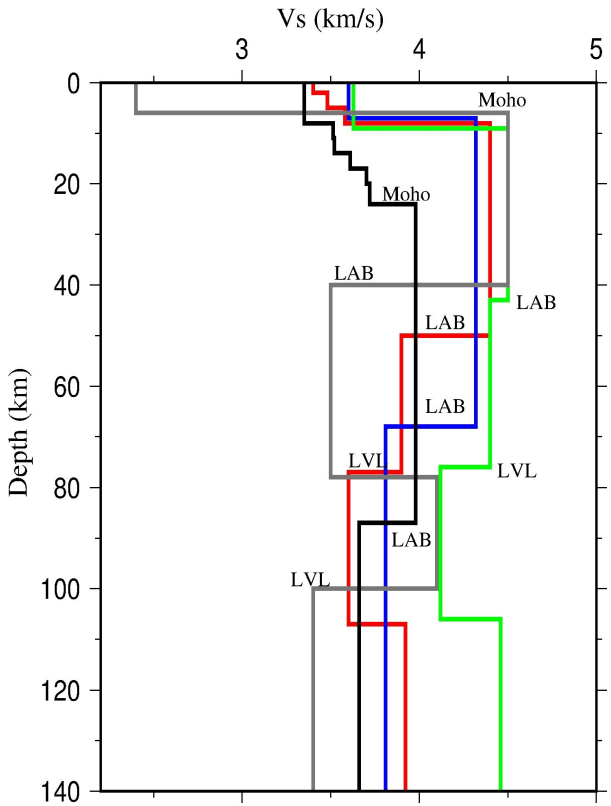

Fig. 3. Shear wave velocity models for different stations that produce a good fit between the synthetic and observed seismograms. Only the upper part of models down to a depth of 140 km containing three discontinuities, Moho, LAB, and LVL are shown. Phases that are above the 2 sigma error limits are modeled. The color codes correspond to different stations: Black- MCQ, Red-ASCN, Blue- PSCM, Green-RPN and Grey-ROSA.

SED
5, 1641–1657, 2013

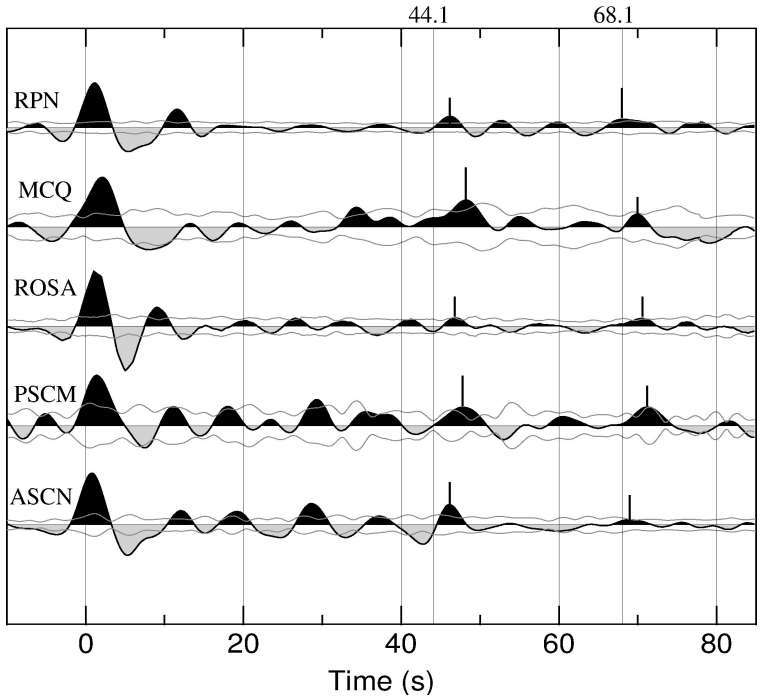

Fig. 4. Stacked receiver functions similar to the Fig. 2 but shown till deeper depths in order to show the upper mantle discontinuities. The traces are low-pass filtered with corner frequency of 6 s and moveout corrected to a reference slowness of 6.4 s deg^{-1} using the IASP91 Earth model prior to stacking. Two bounding lines parallel to the mean are error bounds of ±2 SE. All the stations show clear arrivals of the Ps conversions from the 410 and 660 km discontinuities (marked by short line) and they are delayed with respect to the average global mode.

SED
5, 1641–1657, 2013